

Minimal effect of stacking number on intrinsic cleavage and shear behavior of $\text{Ti}_{n+1}\text{AlC}_n$ and $\text{Ta}_{n+1}\text{AlC}_n$ MAX phases

Cite as: J. Appl. Phys. **123**, 225102 (2018); <https://doi.org/10.1063/1.5026323>

Submitted: 18 February 2018 . Accepted: 24 May 2018 . Published Online: 11 June 2018

 Woongrak Son, Thien Duong,  Anjana Talapatra, Evan Prehn, Zeyi Tan, Miladin Radovic, Raymundo Arróyave, et al.



View Online



Export Citation



CrossMark

ARTICLES YOU MAY BE INTERESTED IN

Experimental and theoretical characterization of ordered MAX phases $\text{Mo}_2\text{TiAlC}_2$ and $\text{Mo}_2\text{Ti}_2\text{AlC}_3$

Journal of Applied Physics **118**, 094304 (2015); <https://doi.org/10.1063/1.4929640>

Intrinsic defect processes and elastic properties of Ti_3AlC_2 (A = Al, Si, Ga, Ge, In, Sn) MAX phases

Journal of Applied Physics **123**, 025103 (2018); <https://doi.org/10.1063/1.5011374>

Electrical and thermal conductivity of the Ti_3AlC_2 MAX phase at low temperatures

Low Temperature Physics **44**, 451 (2018); <https://doi.org/10.1063/1.5034158>

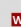
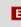
HIDEN
ANALYTICAL

Instruments for Advanced Science

- Knowledge,
- Experience,
- Expertise

Click to view our product catalogue

Contact Hiden Analytical for further details:

 www.HidenAnalytical.com
 info@hiden.co.uk



Gas Analysis

- dynamic measurement of reaction gas streams
- catalysis and thermal analysis
- molecular beam studies
- dissolved species probes
- fermentation, environmental and ecological studies



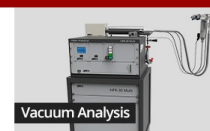
Surface Science

- UHVTPD
- SIMS
- end point detection in ion beam etch
- elemental imaging - surface mapping



Plasma Diagnostics

- plasma source characterization
- etch and deposition process reaction kinetic studies
- analysis of neutral and radical species



Vacuum Analysis

- partial pressure measurement and control of process gases
- reactive sputter process control
- vacuum diagnostics
- vacuum coating process monitoring

Minimal effect of stacking number on intrinsic cleavage and shear behavior of $\text{Ti}_{n+1}\text{AlC}_n$ and $\text{Ta}_{n+1}\text{AlC}_n$ MAX phases

Woongrak Son, Thien Duong, Anjana Talapatra, Evan Prehn, Zeyi Tan, Miladin Radovic, and Raymundo Arróyave^{a)}

Department of Materials Science and Engineering, Texas A&M University, College Station, Texas 77843-3123, USA

(Received 18 February 2018; accepted 24 May 2018; published online 11 June 2018)

MAX phases are layered carbides or nitrides with the general formula $\text{M}_{n+1}\text{AX}_n$, which exhibit a unique combination of ceramic- and metal-like properties. The effect of stacking a number (determined by n) remains to be elucidated and *a priori* is not clear whether, for a given chemistry, n significantly changes the intrinsic deformation behavior of these systems. In this work, we have studied the intrinsic deformation behavior of $\text{Ti}_{n+1}\text{AlC}_n$ and $\text{Ta}_{n+1}\text{AlC}_n$ ($n = 1 \dots 5$) using DFT-based calculations. Surprisingly, the results suggest that the stacking number tends to have a minimal effect on the intrinsic mechanical behavior of the systems studied. *Published by AIP Publishing.* <https://doi.org/10.1063/1.5026323>

I. INTRODUCTION

$\text{M}_{n+1}\text{AX}_n$ (MAX) phases are a group of layered, hexagonal compounds, where M_{n+1}X_n layers are interleaved with A layers. M is typically an early transition metal, A is mostly an element of group 13–16 and X is carbon or nitrogen. MAX phases exhibit a unique combination of properties of both metals and ceramics. Like metals, MAX phases are relatively soft and readily machinable with good damage tolerance and thermal shock resistance. In addition, like ceramics, MAX phases are stiff, have low thermal expansion and exhibit good oxidation and chemical resistance.^{1–3}

Depending on the number n , MAX phases have different numbers of MX stacking layers between A layers with different elastic properties. Different stacking numbers have been observed that influence the mechanical properties of MAX phases, such as $\text{Ti}_{n+1}\text{SiC}_n$, upon increasing bulk modulus from 205 GPa ($n = 1$) to 254 GPa ($n = 4$) as n is increased.⁴ Unfortunately, much remain unknown about the mechanical properties of MAX phases, particularly with regard to the stacking number, as only a few MAX phases with $n = 1$ –3 have been synthesized and characterized, while only a couple of high order MAX phases has been investigated.⁵

In order to understand the intrinsic mechanical behavior of layered systems such as MAX phases, one can investigate the relative propensities to undergo cleavage and shear upon application of stress.⁶ The cleavage energy and stress of a material are related to its fracture behavior,⁷ while the response in shear can be evaluated through the generalized stacking fault energy (GSFE) surface, which provides an indication for the resistance of a given material to plastic deformation in a specific slip system.⁸ Understanding the intrinsic resistance to cleavage and shear deformation can provide insights into the brittle/ductile nature of materials, although here we note that the macro-mechanical response

of materials is the result of multi-scale phenomena and that intrinsic mechanical properties discussed herein only partially contribute to the overall mechanical behavior of the material.

This work is motivated by the following question: *What is the effect, if any, of different stacking numbers on the intrinsic deformation behavior in MAX phases.* The motivation for this work is two-fold: first, this specific question has yet to be addressed—to the best of our knowledge—on a systematic manner; second, understanding the cleavage and shear behavior of different $\text{M}_{n+1}\text{AX}_n$ sequences within the same chemistry system (i.e., M, A and X are fixed) can provide valuable information about the parameterization of micro-mechanical models for deformation in these materials.

To make the problem specific, we study the cleavage behavior of $\text{Ti}_{n+1}\text{AlC}_n$ and $\text{Ta}_{n+1}\text{AlC}_n$ ($n = 1, 2, 3, 4$, and 5) under loading mode 1, in which atoms are allowed to relax after a given value of cleavage distance. In addition, we study the shear behavior of $\text{Ti}_{n+1}\text{AlC}_n$ and $\text{Ta}_{n+1}\text{AlC}_n$ ($n = 1, 2, 3, 4$, and 5), in which atoms are allowed to relax after a given value of shear distance with a fixed shear angle. We have selected Ti and Ta as the M elements in the MAX phases under study, given the fact that multiple layers have been synthesized, and therefore some of the results presented in this work could potentially be verified through indirect means, such as nano-indentation experiments.

II. COMPUTATIONAL DETAILS

A. Density functional theory (DFT)

In this work, calculations were performed through density functional theory (DFT),⁹ which is implemented in the Vienna Ab-initio Simulation Package (VASP),¹⁰ with projected augmented wave (PAW) pseudopotentials.¹¹ The Perdew-Burke-Ernzerhof (PBE) approximation was used to account for exchange correlation.¹² A cutoff energy of 533 eV was set for all calculations. The Brillouin zone integrations were performed using a Monkhorst-Pack mesh with

^{a)}Author to whom correspondence should be addressed: rarrayave@tamu.edu. Tel.: +1 979-845-5416. Fax: +1 979-845-3081.

5000 k-points per reciprocal atom. The electronic configurations of titanium, silicon, aluminium, and carbon were chosen to be $[\text{Ar}]3d^34s^1$, $[\text{Ne}]3s^23p^2$, $[\text{Ne}]3s^23p^1$, and $[\text{He}]2p^2$. The relaxations were carried out by allowing a change in the volume with ISIF = 7 flag, allowing a change in the shape with ISIF = 6 flag, allowing a change in atomic positions with ISIF = 3 flag, and a final self-consistent static calculation. For all relaxations, relaxation stops if the total energy change is smaller than 10^{-6} eV with EDIFF = 10^{-6} flag.

B. Cleavage energy

We implemented a cleavage model under loading mode I,⁷ as shown in Fig. 1(a). In this model, two blocks are separated and structural relaxation is allowed during the cleavage process. In particular, the M-A bond is known to be relatively weaker than the M-X bond; hence, M and A layers are the ones that should be cleaved during the cleavage process.¹ Then, cleavage energy at every separation level was calculated through DFT as follows:

$$\Delta E/A = E(z)/A - E(0)/A, \quad (1)$$

where z is the cleavage distance between M and A layers and A is the surface area. The cleavage stress, $\sigma(z)$, is defined as the first derivative of cleavage energy

$$\sigma(z) = \frac{dE}{dz}. \quad (2)$$

The critical stress, σ_c , is the maximum cleavage stress, which is the stress required to break the bonds between M and A layers.

C. Stacking fault energy (SFE)

In a hexagonal close packed structure of the MAX phase, the most active slip system is $\langle 2\bar{1}10 \rangle \{0001\}$ and it can be separated into two partial dislocations, which are $\langle 2\bar{1}10 \rangle \{0001\}$ and $\langle 0\bar{1}10 \rangle \{0001\}$. The orthorhombic supercell and the schematic view of shear deformations (pure affine, simple affine, pure alias, and simple alias) are shown in Fig. 1(b). Under shear, a crystal structure can be deformed under two distinct deformation modes: affine and alias.⁸ Under affine shear transformation, all atoms are shifted

parallel to the shearing direction by a distance proportional to their distance to a fixed reference basal plane, while under alias transformation, only the top layer of the crystal is displaced in the shear direction. Under alias deformation, the displacement of the top layer and relaxation under fixed displacement of this layer lead to top \rightarrow down propagation of the shear deformation. This mechanism has been deemed to be a more realistic approximation to shear⁸ as it allows the formation of stacking faults.

For both affine and alias transformations, we considered further two possible variants of shear, namely pure and simple.⁸ Under simple shear, shear deformation is not followed by relaxation of the shape of the deformed cell or of the atomic positions. On the other hand, under pure shear, the cell is fully relaxed under the constraint that the shearing angle is fixed. This causes all the components of the stress tensor σ_{ij} to vanish, except for the components associated with the specific shear deformation under consideration, i.e., σ_{13} and σ_{23} . We would like to note that this mode of deformation always corresponds to the minimum energy path along a macroscopic (crystal-level) shear deformation process.

We would like to note that conventional DFT codes do not allow for the constrained relaxation as prescribed by the pure shear deformation. To address this issue, we used the external optimizer GADGET developed by Bucko and collaborators.¹³ This optimizer takes the interatomic forces as calculated by VASP and relaxes the entire cell (including ionic positions) subjected to arbitrary constraints. In this case, we set the shear angle as constant and then relaxed the rest of the cell until all components of the stress tensor (except for those that correspond to specific shear deformation) vanished.

In previous work, the shear deformation behavior of $\text{Ti}_3(\text{Si}_x\text{Al}_{1-x})\text{C}_2$ has been investigated under both $\langle 2\bar{1}10 \rangle \{0001\}$ and $\langle 0\bar{1}10 \rangle \{0001\}$ shear deformations.¹⁴ Those results showed that alias shear deformation along the $\langle 2\bar{1}10 \rangle$ direction is the most preferable shear deformation mechanism as it corresponds to the mechanisms that exhibit the lowest energy barrier. Hence, in this work, we study alias shear deformation of $\text{Ti}_{n+1}\text{AlC}_n$ and $\text{Ta}_{n+1}\text{AlC}_n$ along the $\langle 2\bar{1}10 \rangle$ direction.

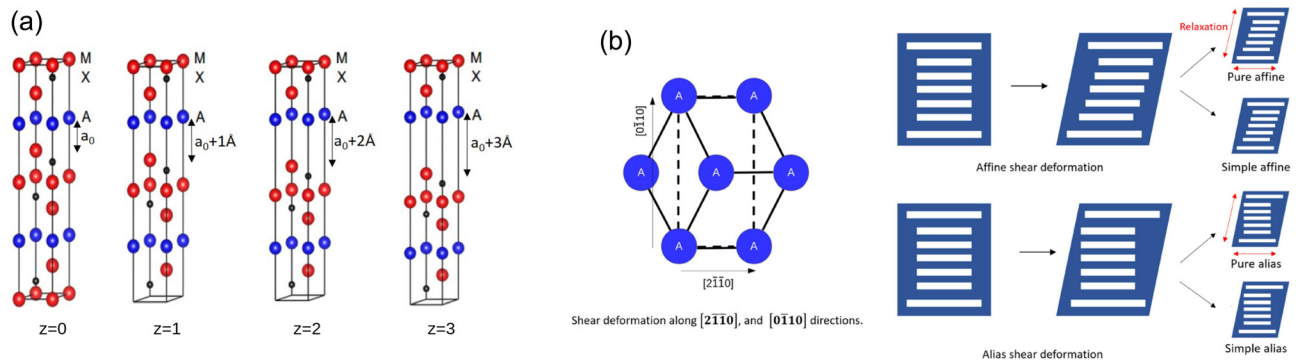


FIG. 1. (a) Schematic of the cleavage between M and A layers under loading mode I. (b) The orthorhombic supercell (dashed line) and the schematic view of pure affine, simple affine, pure alias, and simple alias shear deformations. Reproduced with permission from Ref. 8. (a) Cleavage deformation. (b) Shear deformation.

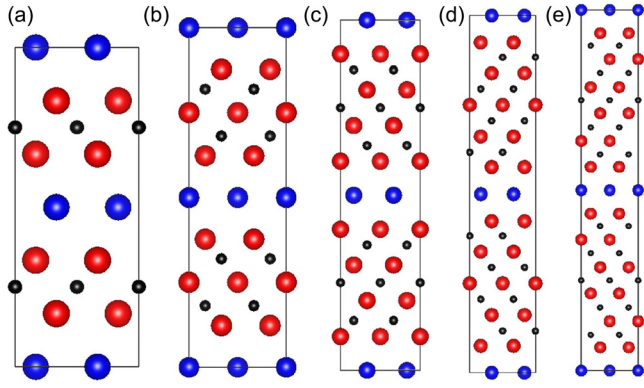


FIG. 2. Crystal structure of $\text{Ti}_{n+1}\text{AlC}_n$ ($\text{Ta}_{n+1}\text{AlC}_n$) with (a) $n = 1$, (b) $n = 2$, (c) $n = 3$, (d) $n = 4$, and (e) $n = 5$. Red, blue, and black atoms represent Ti (Ta), Al, and C, respectively.

III. RESULTS AND DISCUSSION

A. Structural properties

The optimized structure of nano-layered $\text{Ti}_{n+1}\text{AlC}_n$ and $\text{Ta}_{n+1}\text{AlC}_n$ is shown in Fig. 2, using the visualization program VESTA.¹⁵ The calculated a- and c-lattice parameters are shown in Table I, which agree well with other calculated and experimental results.⁵ Both a- and c-lattice parameter values of $\text{Ta}_{n+1}\text{AlC}_n$ are higher than those of $\text{Ti}_{n+1}\text{AlC}_n$. In addition, with increasing number of stacking layers and increasing number of n , the a-lattice parameter is almost constant, while the c-lattice parameter increases. This intuitively makes sense and points to the relative insensitivity of structural parameters to specific stacking

TABLE I. The a- and c-lattice parameter values of $\text{Ti}_{n+1}\text{AlC}_n$ and $\text{Ta}_{n+1}\text{AlC}_n$ ($n = 1, 2, 3, 4$, and 5) in units of Å.

Phase	Ti_2AlC	Ti_3AlC_2	Ti_4AlC_3	Ti_5AlC_4	Ti_6AlC_5
a	3.069	3.082	3.085	3.085	3.084
c	13.734	18.652	23.588	28.541	33.505
Phase	Ta_2AlC	Ta_3AlC_2	Ta_4AlC_3	Ta_5AlC_4	Ta_6AlC_5
a	3.092	3.099	3.136	3.130	3.145
c	13.951	19.252	24.261	29.546	34.550

number, indicating strong localization of the bonding within the M-A layers.

B. Cleavage energy

In $\text{Ti}_{n+1}\text{AlC}_n$ and $\text{Ta}_{n+1}\text{AlC}_n$ systems, we present the cleavage energy and stress calculations as a function of stacking number n , as an indirect measure of the bonding strength between M and A layers. The results of the calculated cleavage energy and stress are shown in Fig. 3. As is shown in Figs. 3(a) and 3(c), the cleavage energy sharply increases in all cases up to around 1 Å of separation, after which its rate of increase decays and in fact saturates at about 3 Å. The cleavage stress is derived from the cleavage energy, and is shown in Figs. 3(b) and 3(d). The maximum cleavage energy (critical stress) appears at around 0.9 Å of separation. The critical stress of $\text{Ti}_{n+1}\text{AlC}_n$ is 23.88, 22.65, 22.55, 22.51, and 22.46 GPa with $n = 1, 2, 3, 4$, and 5 , respectively, while the critical stress of $\text{Ta}_{n+1}\text{AlC}_n$ is 28.33,

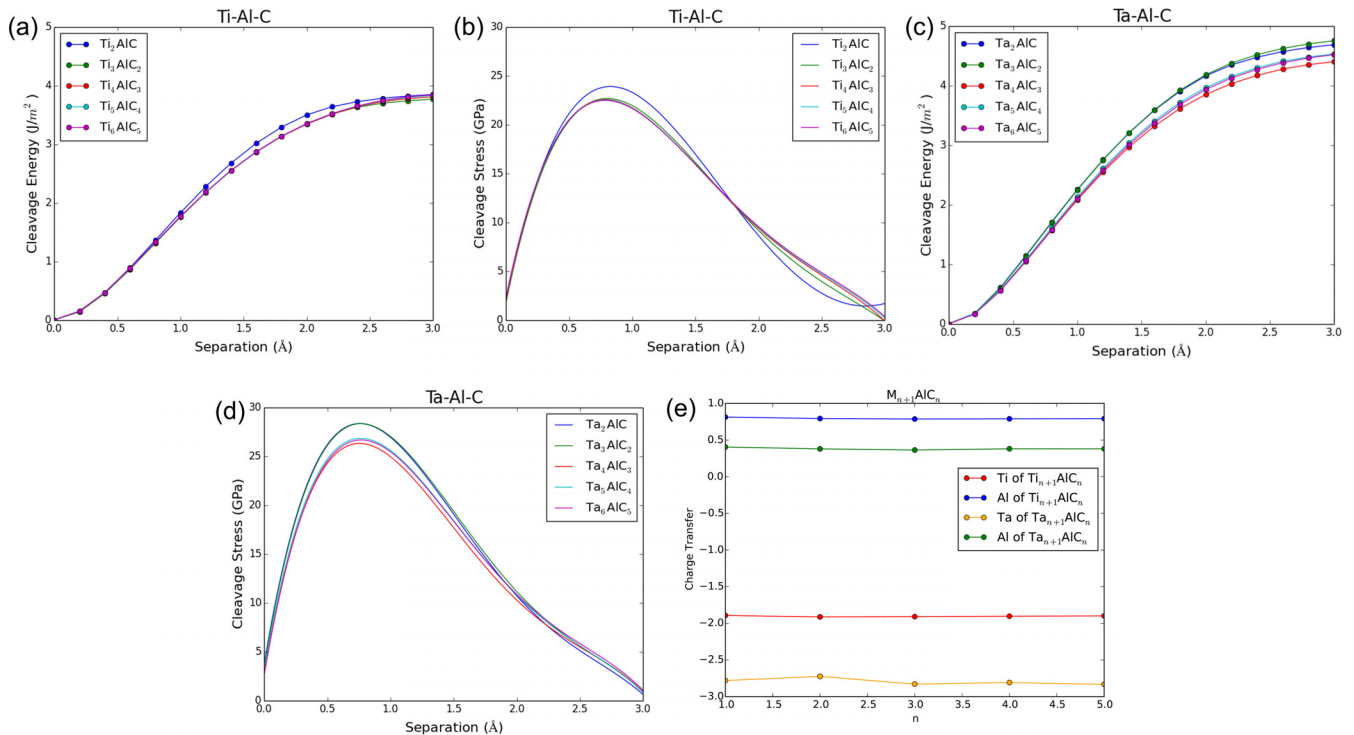


FIG. 3. Cleavage energy and stress of (a and b) $\text{Ti}_{n+1}\text{AlC}_n$ and (c and d) $\text{Ta}_{n+1}\text{AlC}_n$ with $n = 1, 2, 3, 4$, and 5 . (e) Charge transfer of Ti, Ta, and Al of $\text{M}_{n+1}\text{AlC}_n$ ($\text{M} = \text{Ti}$ and Ta). (a) Cleavage energy of $\text{Ti}_{n+1}\text{AlC}_n$. (b) Cleavage stress of $\text{Ti}_{n+1}\text{AlC}_n$. (c) Cleavage energy of $\text{Ta}_{n+1}\text{AlC}_n$. (d) Cleavage stress of $\text{Ta}_{n+1}\text{AlC}_n$. (e) Charge transfer of $\text{M}_{n+1}\text{AlC}_n$.

TABLE II. Calculated number of valence electrons (charge transfer) in $Ti_{n+1}AlC_n$ and $Ta_{n+1}AlC_n$ obtained by Bader analysis.¹⁶ Particularly, the charge analysis of Ti, Ta, and Al in cleaved layers.

Phase	Ti_2AlC	Ti_3AlC_2	Ti_4AlC_3	Ti_5AlC_4	Ti_6AlC_5
Ti	2.107 (−1.893)	2.087 (−1.913)	2.091 (−1.909)	2.097 (−1.903)	2.101 (−1.899)
Al	3.813 (+0.813)	3.794 (+0.794)	3.787 (+0.787)	3.79 (+0.79)	3.792 (+0.792)
Phase	Ta_2AlC	Ta_3AlC_2	Ta_4AlC_3	Ta_5AlC_4	Ta_6AlC_5
Ta	2.22 (−2.78)	2.276 (−2.724)	2.171 (−2.829)	2.192 (−2.808)	2.167 (−2.833)
Al	3.405 (+0.405)	3.38 (+0.38)	3.364 (+0.364)	3.381 (+0.381)	3.38 (+0.38)

28.32, 26.29, 26.81, and 26.65 GPa with $n = 1, 2, 3, 4$, and 5 , respectively.

The critical stress of $Ta_{n+1}AlC_n$ is higher than the critical stress of $Ti_{n+1}AlC_n$, while the number of stacking layers (number of n) does not significantly affect the critical stress. The slight changes in critical stresses in $Ti_{n+1}AlC_n$ and $Ta_{n+1}AlC_n$ systems with different number of stacking layers can be explained by the charge transfer of Ti, Ta, and Al in cleaved layers, and are shown in Table II and Fig. 3(e). In the $Ti_{n+1}AlC_n$ system, the calculated charge transfer of Ti is −1.893, −1.913, −1.909, −1.903, and −1.899, and that of Al is 0.813, 0.794, 0.787, 0.79, and 0.792 with $n = 1, 2, 3, 4$, and 5 , respectively. In $Ta_{n+1}AlC_n$, the calculated charge transfer of Ta is −2.78, −2.724, −2.829, −2.808, and −2.833, and the calculated charge transfer of Al is 0.405, 0.38, 0.364, 0.381, and 0.38 with $n = 1, 2, 3, 4$, and 5 , respectively. The charge transfer of Ti, Ta, and Al changes by about 1% at most with changing n , providing a rationalization for the fact that the critical cleavage stress in $Ti_{n+1}AlC_n$ and $Ta_{n+1}AlC_n$ is insensitive to the stacking number: the strength of the bonding between M and A layers is highly localized within the M-A layers themselves and the stacking number does not affect their interactions.

C. Generalized stacking fault energy (GSFE) calculations

It has been shown in a prior work by the present authors that the alias shear deformation along $\langle 2\bar{1}10 \rangle \{0001\}$ is the most preferable shear deformation,¹⁴ and hence we present energy curves under $\langle 2\bar{1}10 \rangle \{0001\}$ alias shear deformation.

The energetics of $Ti_{n+1}AlC_n$ under simple shear deformations by shearing M-X and M-A layers as a function of fraction of the Burgers vector are shown in Fig. 4(a). The resultant energies for the simple alias calculation by shearing M-X layers are much higher than those corresponding to the simple alias calculation by shearing M-A layers. This shows that the number of stacking layers significantly affects the resultant energies under simple alias deformation by shearing M-X layers, which corresponds to the energy required to slip M and X layers. The energetics of simple alias calculations without and with atomic relaxation and pure alias calculation are shown in Fig. 4(b). The resultant energies of the simple alias calculations are much higher than those corresponding to the pure alias calculation. The reason for this considerable overestimation is the fact that atomic relaxations consistent with the shear deformation of the cell must be taken into account in order to minimize the total strain energy of the system. We note, however, that carrying out a simple alias shear, but allowing at least local ionic relaxations is sufficient to reduce the energy barrier to shear to values close to those obtained using the pure shear construction. Note, however, that when carrying out the pure shear transformation, no assumption as to the identity of the sheared layers had to be made as this is a direct outcome of the constrained relaxation scheme.

The energetics of shear deformation for $Ti_{n+1}AlC_n$, and $Ta_{n+1}AlC_n$ are shown in Figs. 5(a), 5(b), 5(c), and 5(d). The unstable stacking fault energy (USFE) is the maximum energy during the shear process, which is the required energy for the generation of stacking fault and can be related to the

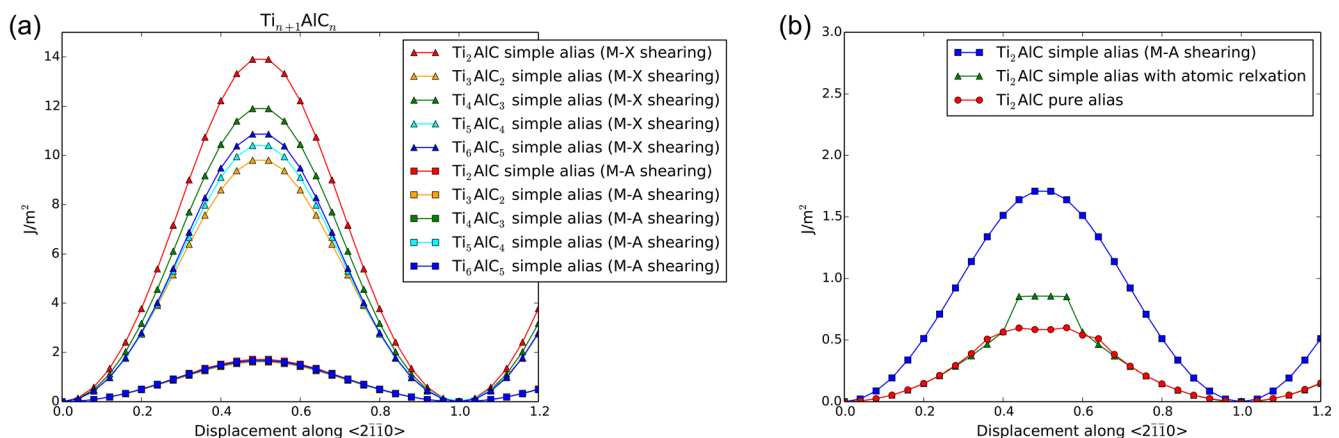


FIG. 4. (a) Simple alias shear deformation energy curves of $Ti_{n+1}AlC_n$ by shearing M-X (triangle) and M-A (square) layers with $n = 1-5$. (b) Shear energy curves of Ti_2AlC under simple alias without (square) and with (triangle) atomic relaxation and pure alias (circle) shear deformation. (a) $Ti_{n+1}AlC_n$, (b) Ti_2AlC .

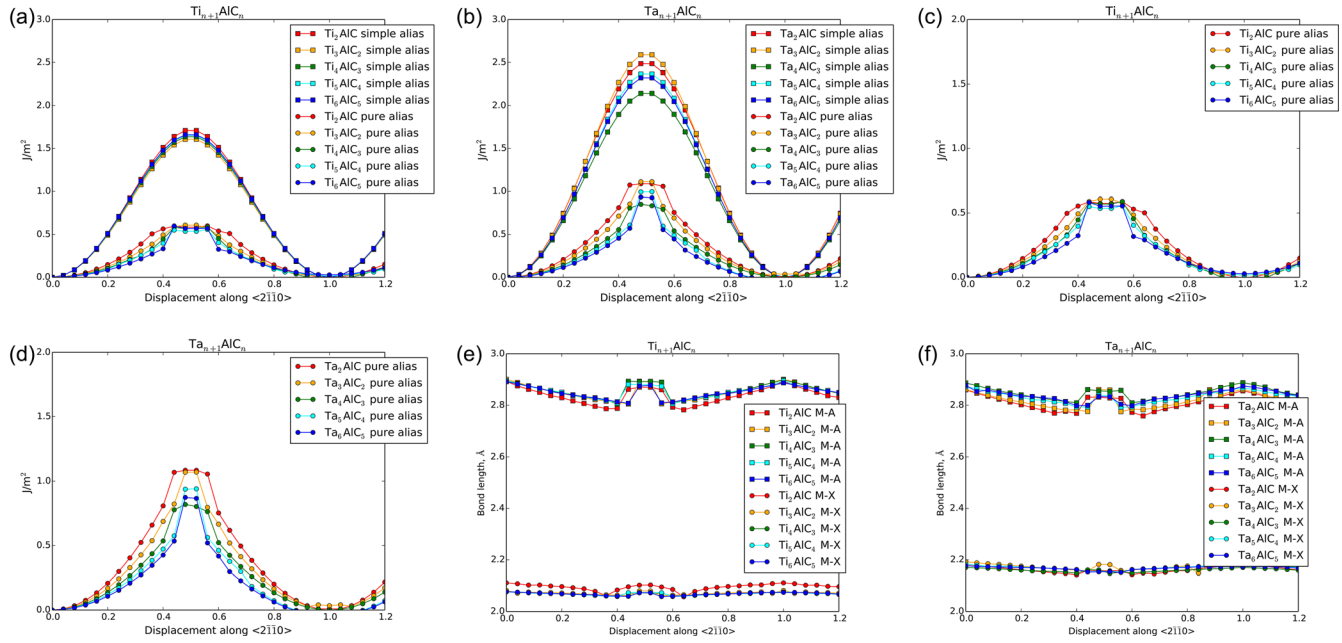


FIG. 5. Shear energy curves of (a) $Ti_{n+1}AlC_n$ and (b) $Ta_{n+1}AlC_n$ with $n=1-5$. Pure alias shear energy curves of (c) $Ti_{n+1}AlC_n$ and (d) $Ta_{n+1}AlC_n$ with $n=1-5$. M-A and M-X bond lengths of (e) $Ti_{n+1}AlC_n$ and (f) $Ta_{n+1}AlC_n$ with $n=1-5$.

required energy for the nucleation of dislocation.⁶ In the $Ti_{n+1}AlC_n$ system, the USFE is 0.588, 0.607, 0.589, 0.556, and 0.555 J/m² with $n=1, 2, 3, 4$, and 5, respectively. In the $Ta_{n+1}AlC_n$ system, the USFE is 1.084, 1.070, 0.818, 0.940, and 0.873 J/m² with $n=1, 2, 3, 4$, and 5, respectively.

The USFE of $Ta_{n+1}AlC_n$ is considerably higher than that of $Ti_{n+1}AlC_n$, while the number of stacking layers does not significantly affect the USFE, which is consistent with the findings derived from the cleavage calculations. Here, we note that the same conclusion would not have been arrived at if one were to consider shear deformation of these systems under simple alias deformation, which would predict differences of more than 30% in the calculated values for the USFE in the case of Ta-MAX phases. Moreover, the results show that the stacking fault is generated between M and A layers, not M and X layers, with the former pair being the most weakly bonded of the two, as M-X bonds tend to be covalent in nature and are much stronger than the predominantly metallic M-A bonds. Again, the generation of the stacking fault is highly localized and is thus reasonable that the number of stacking layers does not affect the USFE. The difference between Ti- and Ta-MAX phases, however, points to the significant effect of chemistry on the strength between M and A layers in MAX phases.

To better understand the slip between M and A layers under shear deformation, the bond lengths of M-A and M-X were calculated and shown in Figs. 5(e) and 5(f). It has been shown that the USFE occurs when the shear deformation has reached a magnitude of about 0.4 Burgers vector and stacking fault is generated at this point, as the system is unstable and incapable of resisting the formation of this stacking defect. The figure indicates that just before the generation of the stacking fault, the bond lengths of M-A and M-X decrease linearly. The decrease in the M-A bond length is thus associated with a considerable increase in the GSFE

profile as the structure is being sheared. At the displacement level corresponding to the point at which the stacking fault is generated, the M-A bond length increases sharply by about 2%, while the M-X bond length increases in a more parsimonious manner, indicating that the M-X layers are not affected significantly by the formation of the stacking fault. This figure shows that the stacking fault is dominated by the slip between the M and A layers.

To justify the unit cell alone is sufficient to achieve reasonable stacking fault energies, we studied pure alias shear deformation of Ti_2AlC with different system sizes. We studied the pure alias shear deformation along $\langle 2\bar{1}\bar{1}0 \rangle \{0001\}$ of Ti_2AlC with a single unit cell and two unit cells in out of plane, and is shown in Fig. 6. Both the single unit cell and the extended unit cell show the maximum energy, USFE, at 40% of displacement. The USFE of the single unit cell and

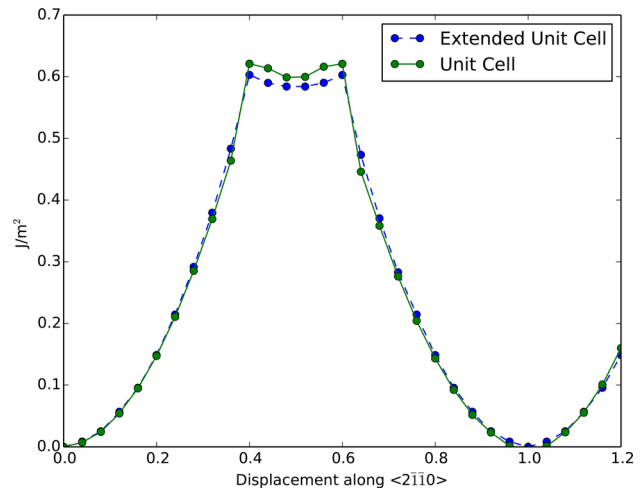


FIG. 6. Shear energy curves of the Ti_2AlC system with one single unit cell (solid line) and two unit cells in out of plane (dashed line).

the extended unit cell are 0.60 and 0.62 J/m², respectively. The calculated USFE of different cell sizes suggests that the system size does not significantly affect the results of shear energy, and thus the single unit cell is sufficient to study shear behavior and achieve reasonable stacking fault energy.

IV. CONCLUSIONS

As mentioned above, this study was motivated by the question of whether the stacking layer number in MAX phases played a fundamental role in their intrinsic mechanical behavior as manifested in their resistance to cleave or shear. Our results suggest that in fact there is no significant effect of layer number on the cleavage energy and stress, which can be rationalized by the fact that the strength (or lack thereof) of the bonding between the M and A layers is localized within the M-A bonds, with minimal influence from the rest of the layers in the crystal. The differences are, however, observed when comparing Ti- and Ta-based MAX systems, indicating a noticeable chemical effect.

Our predictions for the resistance of the materials to shear suggest, once again, that in these layered systems, the stacking number does not play an important role when it comes to predicting the magnitude of the USFE. However, the chemistry was found to play a very significant role, with Ta_{n+1}AlC_n having an USFE about 60% larger than that of Ti_{n+1}AlC_n. This is notable, as it may have important implications on the mechanical response of these systems. Here, we note once again that this conclusion could not have been arrived at if we had to use the simple mode for shear deformation as in this case the cells and ions are not fully relaxed and the resistance to shear is highly overestimated.

While the results here are not generalizable, they suggest that the stacking layer number is not an important factor in determining the intrinsic mechanical properties of MAX phases. While this is not surprising *a posteriori*, given the highly localized nature of the weakest motif in the crystal structure (i.e., M-A layers), the results could not have been arrived at had we used an incorrect assumption as to the nature of atomic relaxations associated with the shear deformation in MAX phases. These results provide further insights into and contribute to the development of a better understanding of the micro-mechanics of deformation in MAX phases, although we admit that the latter is the result of complex, multi-scale features and phenomena that are not captured with the crystal-level calculations carried out in this work.

ACKNOWLEDGMENTS

We acknowledge the support from the NSF Grant Nos. DMR-1410983 and CMMI-1729350 (DMREF). R.A. and A.T. acknowledge partial support from the Grant AFOSR-FA9550-16-1-0180. R.A., M.R., and E.P. would also like to acknowledge the support of the National Science Foundation through Grant No. NSF-DGE-1545403 (NSF-NRT Data-Enabled Discovery and Design of Energy Materials). First-principles calculations were carried out at the Texas A&M Supercomputing Facility in Texas A&M University.

- ¹M. W. Barsoum, *MAX Phases: Properties of Machinable Ternary Carbides and Nitrides* (John Wiley & Sons, 2013).
- ²M. Radovic and M. W. Barsoum, "Max phases: Bridging the gap between metals and ceramics," *Am. Ceram. Soc. Bull.* **92**(3), 20–27 (2013).
- ³M. W. Barsoum, "The MN+1AX_n phases: A new class of solids: Thermodynamically stable nanolaminates," *Prog. Solid State Chem.* **28**(1–4), 201–281 (2000).
- ⁴J.-P. Palmquist, S. Li, P. Å. Persson, J. Emmerlich, O. Wilhelmsson, H. Högborg, M. Katsnelson, B. Johansson, R. Ahuja, O. Eriksson *et al.*, "Mn+1AX_n phases in the Ti-Si-C system studied by thin-film synthesis and ab initio calculations," *Phys. Rev. B* **70**(16), 165401 (2004).
- ⁵Z. Sun, "Progress in research and development on max phases: A family of layered ternary compounds," *Int. Mater. Rev.* **56**(3), 143–166 (2011).
- ⁶P. Lazar and R. Podloucky, "Ab initio study of the mechanical properties of NiAl microalloyed by X = Cr, Mo, Ti, Ga," *Phys. Rev. B* **73**(10), 104114 (2006).
- ⁷P. Lazar and R. Podloucky, "Cleavage fracture of a crystal: Density functional theory calculations based on a model which includes structural relaxations," *Phys. Rev. B* **78**(10), 104114 (2008).
- ⁸M. Jahnátek, J. Hafner, and M. Krajčí, "Shear deformation, ideal strength, and stacking fault formation of fcc metals: A density-functional study of Al and Cu," *Phys. Rev. B* **79**(22), 224103 (2009).
- ⁹W. Kohn and L. J. Sham, "Self-consistent equations including exchange and correlation effects," *Phys. Rev.* **140**(4A), A1133 (1965).
- ¹⁰G. Kresse and J. Furthmüller, "Efficient iterative schemes for ab initio total-energy calculations using a plane-wave basis set," *Phys. Rev. B* **54**(16), 11169 (1996).
- ¹¹J. P. Perdew, K. Burke, and Y. Wang, "Generalized gradient approximation for the exchange-correlation hole of a many-electron system," *Phys. Rev. B* **54**(23), 16533 (1996).
- ¹²M. Ernzerhof and G. E. Scuseria, "Assessment of the Perdew–Burke–Ernzerhof exchange-correlation functional," *J. Chem. Phys.* **110**(11), 5029–5036 (1999).
- ¹³T. Bučko, J. Hafner, and J. G. Ángyán, "Geometry optimization of periodic systems using internal coordinates," *J. Chem. Phys.* **122**(12), 124508 (2005).
- ¹⁴W. Son, H. Gao, T. Duong, A. Talapatra, M. Radovic, and R. Arróyave, "Effect of a mixing on elastic modulus, cleavage stress, and shear stress in the Ti₃(Si_xAl_{1-x})C₂ max phase," *Phys. Rev. B* **95**(23), 235131 (2017).
- ¹⁵K. Momma and F. Izumi, "Vesta: A three-dimensional visualization system for electronic and structural analysis," *J. Appl. Crystallogr.* **41**(3), 653–658 (2008).
- ¹⁶G. Henkelman, A. Arnaldsson, and H. Jónsson, "A fast and robust algorithm for bader decomposition of charge density," *Comput. Mater. Sci.* **36**(3), 354–360 (2006).